Journal of Nano Research
ISSN: 1661-9897, Vol. 63, pp 47-63
doi:10.4028/www.scientific.net/JNanoR.63.47

Submitted: 2019-12-11
Accepted: 2020-05-04
Online: 2020-06-10

Nanocomposite Synthesis from a Natural Clay-Rich Soils and Exhausted Coffee Grounds for Environmental Applications

Vianey Urdapilleta-Inchaurregui[1,a], Fabián Fernández-Luqueño[2,b*], Aidé Minerva Torres-Huerta[3,c], Daniela Roa-Velázquez[1,d], Francisco Javier Rodríguez-Varela[2,e] and María Esther Sánchez-Castro[2,f]

[1]Programa de Nanociencias y Nanotecnología, Cinvestav, Av. Instituto Politécnico Nacional 2508, Ciudad de México, 07000, México

[2]Sustainability of Natural Resources and Energy Programs, Cinvestav-Saltillo, Av. Industria Metalúrgica 1062, Parque Industrial Saltillo-Ramos Arizpe, Ramos Arizpe, Coahuila, 25900, Mexico

[3]Instituto Politécnico Nacional, UPII Hidalgo, Carretera Pachuca-Actopan km 1+500, Pachuca Cd del Conocimiento y la Cultura, San Agustín Tlaxiaca, 42162 Hidalgo, México.

[a]vurdapilletas@cinvestav.mx, [b]cinves.cp.cha.luqueno@gmail.com, [c]atorresh@ipn.mx, [d]daniela.roa@cinvestav.mx, [e]javier.varela@cinvestav.edu.mx, [f]esther.sanchez@cinvestav.edu.mx

Keywords: antimicrobial; environmental pollution; nanoremediation; natural soil; photocatalytic; photodegradation; remediation; surface area; water treatment.

Abstract. Natural clays, engineered Ag-nanoparticles (NP), TiO_2-NP, and exhausted coffee grounds were used to synthesize a nanocomposite 7NC using a Vertisol soil through a single-step by thermal method, to build a nanomaterial to degrade or filtrate pollutants from soils, water or air. The surface characteristics and the porosity of the composite were studied through nitrogen gas adsorption at liquid nitrogen temperature and application of the Brunauer–Emmett–Teller (BET) equation and the results indicated that the microporous composites ranged a surface area of 17.36 m^2 g^{-1}. X-ray diffraction showed crystalline structure and crystalline phase of the nanocomposites. HR-TEM-STEM results demonstrated that TiO_2-NP surrounded Ag-NP, and both were impregnated on natural soil nanoparticles. Oxidation states of the Ag-NP and TiO_2-NP were analyzed by X-ray photoelectron spectroscopy (XPS) The energy gap of nanocomposite 7NC was determined using the Kubelka-Munck model from Ultraviolet–visible diffuse reflectance (UV–Visible DRS) spectra. The photocatalytic activity of these nanocomposites was evaluated, and the results indicated that nanocomposite with Vertisol-soil-NP (7NC) degraded the harmful organic compound methylene blue (MB) while the antimicrobial activity and resistance against Escherichia coli and Staphylococcus aureus and the zone of inhibition (ZOI) also were analyzed. The nanocomposites Ag-NP/TiO_2-NP/natural-soil-NP/exhausted coffee-ground showed its for the development of an efficient material for environmental remediation with photocatalytic and antimicrobial activity.

Introduction

Currently, the water pollutants include complex xenobiotic substances, known as emerging contaminants (ECs), along with organic matter and microorganisms [1]; all of these contaminants have been sensed in drinking water sources, increasing the hazards of illness as a result of intake unclean water [2]. There are different techniques of removal treatments to dissipate contaminants such as coagulation-flocculation, activated carbon adsorption (ACs), ozonation, advanced oxidation processes (AOPs), membrane processes, and membrane bioreactor, among others.

However, the adsorbent synthesis methods must be evaluated because they could change the usage time, particle size, and morphology. At the same time, they must be analyzed for the physicochemical properties of EC to know if adsorbents can chelate them. Besides, the reuse and regeneration of adsorbents should be monitored, making them environmentally friendly [3].

Some nanoparticles, such as TiO_2-NP, Ag-NP, or soil clays, have been used in environmental decontamination [4]. TiO_2 has been identified as one of the semiconductors with a high photocatalytic

capacity owed to its attractive advantages, such as lower cost, high activity, and chemical stability [5]. One strategy for water purification involves photocatalysts with semiconducting properties such as TiO_2. Therefore, TiO_2-NP have been studied in the field of photocatalysis, but these metal oxide can be excited only under UV light irradiation due to their bandgap, i.e., there are some obvious deficiencies such as large band gap and fast recombination of photogenerated e−-h+ pairs restricted the practical application of TiO_2 as photocatalyst.

To counteract the deficiencies of metal oxide have been proposed methods including metal deposition, doping with metals and non-metals, or coupling with other metal oxides with narrower band gaps that methods have been proved to be valid for modification of TiO_2. Other factor critics on the photocatalytic properties of TiO_2 is the number of surface-active sites that depends on surface area and crystal structure characteristics. It is reported that a larger surface area and higher crystallinity are conducive to benefit the surface photocatalytic reaction [6]. There is another form to combine the TiO_2 with clays; these allow the incorporation of noble metal NPs (Pd, Pt, Ag) and could perform their efficiency as photocatalysts through the modification in its structure. The Ag has been known by their antimicrobial properties trough history and Ag-NP by their excellent catalytic efficiency because can facilitate the electron transfer, but Ag-NP could damage the environment. Therefore, the nanocomposite Ag- TiO_2- NP could enhance the photocatalytic degradation of various organic pollutants [7] but without collateral damage to the environment.

Several researchers have reported on the synthesis of Ag and TiO_2 recently. Wu et al. [8] and Poo-arporn et al. [9], studied the changes of crystalline structure through the chemical modification by thermal method and calcination technique for enhancing the visible light photocatalytic activity and their findings have been taken into account in this research, while several forms to attach the Ag-NP and TiO_2-NP into the clay or natural soils have also been reported [10]. The clay minerals advantages over other adsorbents are their relative abundance in nature, cost-effective and environmental friendliness in their applications. Furthermore, they have large specific surface areas, high porosity, surface charge, and surface functional groups, which qualify them as useful adsorbent, that feature allowed to attach the Ag-NP and TiO_2-NP into the layers of clays-NP. Besides, there are some researches of other adsorbents from agricultural wastes such as fruit waste, coconut shell, rice husk, and coffee ground while the study of the capability to remove heavy metals by clays has improved. Therefore, we hypothesize that the combination of TiO_2, Ag, exhausted coffee ground and natural soil will be effective for water purification and environmentally friendly.

The objective of this research was to synthesize and evaluate an Ag-NP/TiO_2-NP/Vertisol soil-NP/exhausted coffee-ground nanocomposite by the thermal method using tetrabutyl titanate and silver nitrate as precursors, and natural soil to build composites with enhanced photocatalytic and antimicrobial activities. The thermal properties of powders, in particular sintering behavior, are influenced by their surface characteristics like specific surface area and pore volume. The structural features of our prepared composites were investigated by using different characterization methods. The surface characteristics of nanocomposites were studied through nitrogen gas adsorption at liquid nitrogen temperature and application of the BET equation. Performances of the nanocomposite materials were evaluated under visible light illumination for the photocatalytic decomposition of methylene blue. These results demonstrate that the Ag-NP/TiO_2-NP/Vertisol soil-NP/exhausted coffee-ground composite exhibited photocatalytic and antimicrobial activity.

Materials

All chemical reagents were of analytical grade and used as received without any further purification. Silver nitrate ($AgNO_3$), tetrabutyl titanate (Titanium(IV) butoxide), Ti $(OCH_2CH_2CH_2CH_3)_4$), ethanol, and methylene blue were purchased to Sigma Aldrich. Deionized water was used in all experiments. The natural Vertisol-soil was sampled in Guanajuato, Mexico. The Gram-negative bacteria *Escherichia coli* and Gram-positive bacteria *Staphylococcus aureus* were purchased from the 'Colección Nacional de Cepas Microbianas y Cultivos Celulares del Cinvestav' at Mexico City and used to test the antimicrobial activity of the built composites.

Preparation of composite of Ag-NP/TiO_2-NP/Vertisol soil-NP/exhausted coffee-ground.

The Ag-NP/TiO_2-NP/Vertisol soil-NP/exhausted coffee-ground nanocomposite was processed by a thermal method and calcinated, is described below.

The natural-soil clays and exhausted coffee ground were mixed and placed into a flask; then, 950 mL of ethanol were poured under continuous stirring until a suspension was achieved. Later, 6.5 g $AgNO_3$ and 30 mL tetrabutyl titanate were added in the suspension and stirred during 2 h. The suspension was placed into a porcelain crucible and heated at 160 ºC for 24 h in a high-temperature oven. The suspension was centrifuged at 7800 rpm and washed with deionized water and ethanol to remove impurities. The precipitate was dried at 60 ºC for 2 h to obtain black powder. Finally, the powder was calcinated at 500 ºC, using a temperature ramp of 5 ºC per minute for twelve hours to obtain a beige powder called 7NC when Vertisol-soil was used (Figure 1).

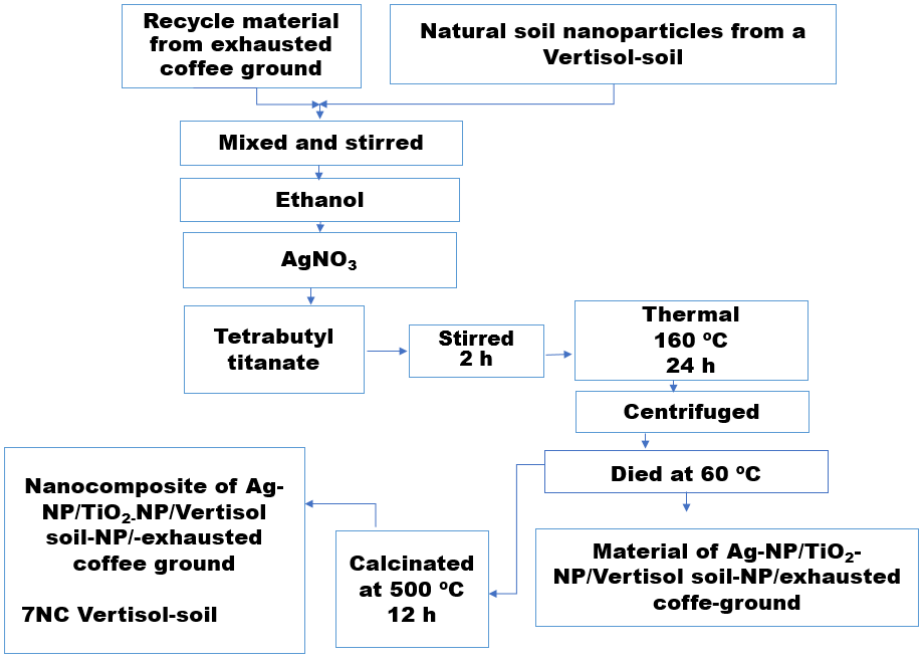

Figure 1. Synthesis method of the nanomaterial with Vertisol-soil (7NC).

Characterization of the composites

The synthesized nanomaterial was characterized by X-ray diffraction (XRD, Smart Lab Rigaku) using the powder configuration, Kα radiation of Cu (λ = 1.5406 Å) and the crystalline phases of the nanomaterials were determined. X-ray diffraction patterns were recorded at 35 kV and 45 mA in the 2θ range of 5° - 80°. The spectral plots were compared with details obtained from the Joint Committee on Powder (JCPDS) for analytical purposes. High-resolution transmission electron microscopy (H-RTEM) and STEM (JEOL 2100) were used to analyze the morphology, and H-RTEM revealed lattice spacings for the compounds. The particle size was determined directly from the images by using the software of the equipment Digital Micrograph Gatan™. The chemical composition properties were recorded using a scanning electron microscopy (SEM) and energy dispersive X-ray spectrometer (EDS) (SEM-EDS, Bruker Zeiss). Light absorption was studied using Agilent Ultra Violet–vis diffuse reflectance (UV-vis DRS) spectrophotometer with an integrating sphere and a spectral reflectance standard over a wavelength range of 200–800 nm and the energy gap of nanomaterials composites was determined using the Kubelka-Munck model. Fourier transform infrared (FT-IR) absorption spectra were recorded by Nicolet 6700 FT-IR instrument. Raman spectra were recorded by NT-MDT INTEGRASpectra using a laser with a 473 nm wavelength as the source and a 600/600 grid. The spectra were traced in the range 3500–50 cm^{-1} with 500 scans at 0.1 cm^{-1} resolutions and, the spectral recordings were carried out at room temperature. Both infrared and Raman analysis permitted the identification of the main molecular groups present in the samples.

The surface compositions of the composites prepared were also analyzed by X-ray photoelectron spectroscopy (XPS) using a Thermo Scientific™ K-Alpha™+X-ray Photoelectron Spectrometer (XPS) System. The binding energy was calibrated by the C1s peak at 284.5 eV.

The surface characteristics, the porosity, and the adsorption-desorption isotherms of the material Ag-NP/TiO_2-NP/Vertisol soil-NP/exhausted coffee-ground produced by thermal method were studied for a standard volumetric method by nitrogen adsorption at 75 K and the BET equation. The measurements were carried out in an ASAP 2050 device. The surface conditions of the 7NC were studied.

Photocatalytic activity test

The photocatalytic performance was constructed on the photocatalytic degradation of the harmful organic pollutant of methylene blue (MB) solutions under exposure to UV light at room temperature. Tablets of Ag-NP/TiO_2-NP/Vertisol soil-NP/exhausted coffee-ground composites were placed into the quartz cell with 3 mL of an aqueous MB solution at 2.5 10^{-5} M concentration. The setup was placed in a box sealed with aluminum foil to keep out external light and equipped with a lamp 40 W and wavelength 232 nm. The UV light sources were then turned on, and this moment was considered as time 0 (t=0) for the degradation reaction. Under environment conditions and stirring, the contents of the quartz cell were exposed at regular intervals to UV light for 150 minutes. The obtained solutions were analyzed using a UV–visible spectrophotometer with a quartz cuvette that has an optical length of one cm. The solution was analyzed following the removal of the photocatalyst. The degradation of the organic pollutant (MB) was determined by using a Spectrophotometer Shimadzu Uv-2401 PC. The 7NC composite was placed in reactor, and the test was carried out for triplicate. After regular time intervals of 30 mins, 3 mL of dye solution was sampled, and its concentration was measured by recording the absorbance corresponding to $\lambda \approx 664$ nm for MB.

Antimicrobial activity

The antimicrobial activity and resistance against *Escherichia coli* and *Staphylococcus aureus* were tested according to EPA (Environmental Protection Agency) by the Antimicrobial Disk Susceptibility method and the Mexican Standard NOM-127-SSA1-1994 [11-13]. Three sets of simultaneous controls were used. The diameters of the inhibition zones (zone of inhibition—ZOI) were measured in millimeters. The replicates, along with the standard error of the mean (sem) were calculated.

Results and Discussion

Morphological and structural characterization

The crystalline structure and crystalline phase composition of the synthesized Ag-NP/TiO_2-NP/Vertisol soil-NP/exhausted coffee-ground was studied by the X-ray diffraction (XRD).

Figure 2 shows the X-ray pattern of the Vertisol soils used in the synthesis; diffractions can be assigned to quartz (SiO_2) (Q), kaolinite (K) ($Al_2(SiO_2O_5)(OH)_4$), mullite (M) ($Al_6Si_2O_{13}$), among others. The assignment to a JCPDS card and diffractions of the phases was difficult because the soils contain a significant part of minerals like quartz, clays, kaolinite, and mullite but, all of them contain Si and O [31,32]. It has to be remembered that the type of soil used in this investigation was chosen for its characteristics and the quantity of clays.

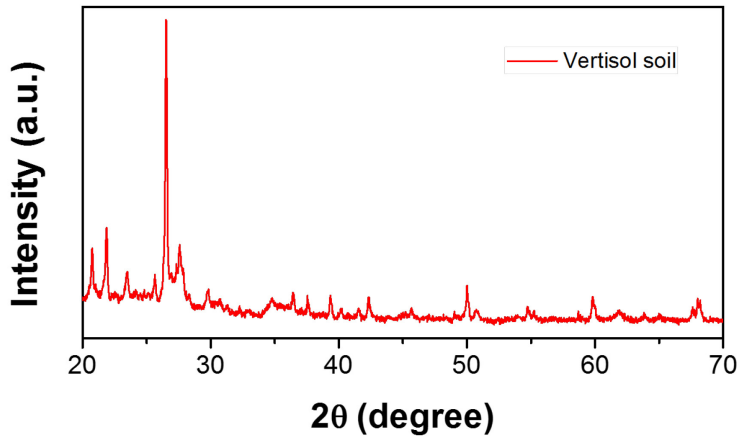

Figure 2. XRD diffraction pattern of a Vertisol-soil.

Figure 3 shows the X-ray pattern of the synthesized composite. The signal located at 2θ = 26º in Figure 2 (Q), can be assigned to the Vertisol-soil which matches with the composite of Ag-NP/TiO_2-NP/Vertisol-soil-NP/exhausted coffee-ground (7NC) (Figure 3b) The reflections located at 38.1º, 44.3º, 64.4º and 77.4º (2θ) can be assigned to the (1 1 1), (2 0 0), (2 2 0) and (3 1 1) planes of the cubic phase of Ag with lattice constant (JCPDS file: 04-0783) from the composite 7NC (Figure 3b). Then, the synthesized material shows the presence of Ag-NP-TiO_2-NP-soil-NP confirming the composite production and that is a nanocomposite.

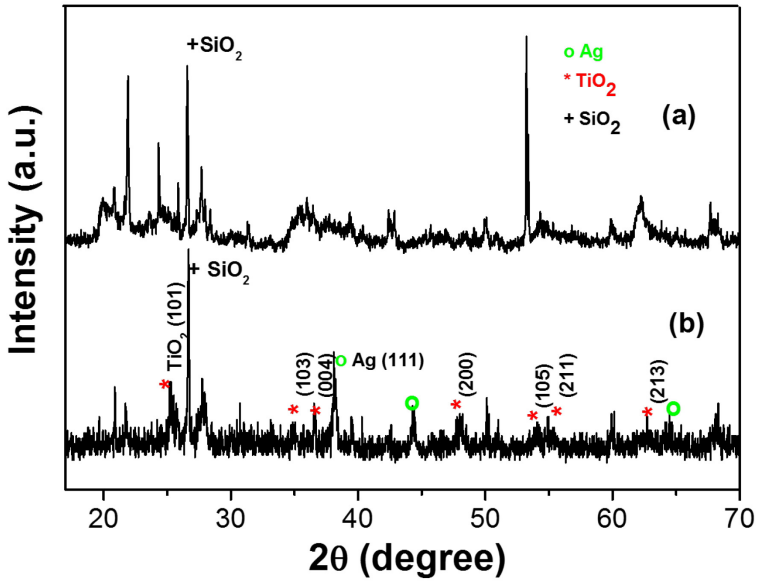

Figure 3. XRD diffraction patterns. (a) Diffractogram of vertisol soil, (b) Diffractogram of the nanomaterial Ag-NP/TiO_2-NP/vertisol-soil-NP/exhausted coffee-ground (7NC).

Figure 4 shows the crystallinity of the materials composite with Vertisol-soil before and after were calcinated. Crystalline and the crystal phase are crucial parameters that determine the photocatalytic activity of TiO_2, where the crystalline anatase phase is considered as the most active form of TiO_2. The synthesized composite with only thermal method display a low crystallinity in comparison to composite obtained with calcination process (Figure 4). It could extend the TiO_2 photoabsorption range from UV to visible light spectrum. Match™ software with refinement of Rietveld method was used to determine the different phases of the composites.

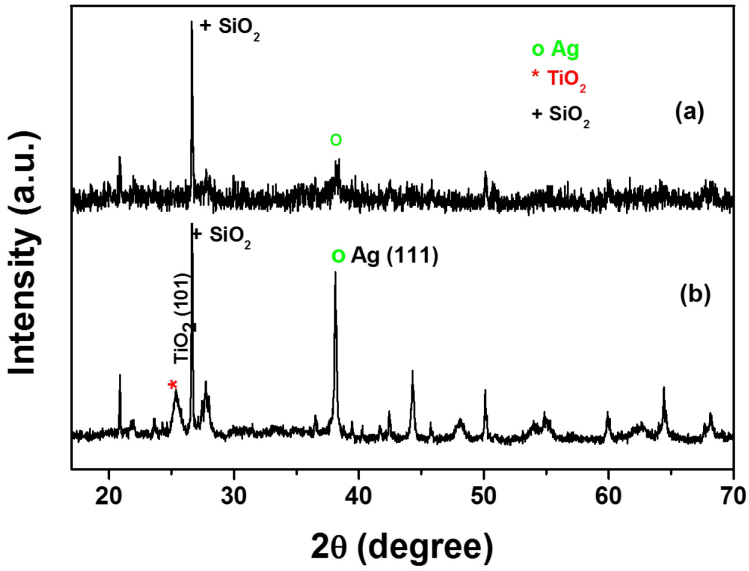

Figure 4. XRD diffraction patterns. (a) Nanocomposite Ag-NP/TiO_2-NP/vertisol-soil-NP/exhausted coffee-ground before calcination, and (b) Nanocomposite Ag-NP/TiO_2-NP/vertisol-soil-NP/exhausted coffee-ground (7NC) calcinated.

Figure 5 shows the cubic Ag phase, anatase TiO_2 phase and hexagonal SiO_2 P phase on sample 7NC synthetized with Vertisol-soil.

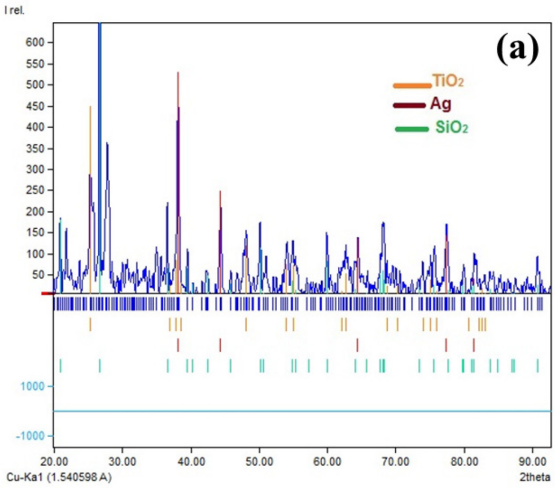

Figure 5. Phases of the nanocomposite 7NC synthesized-calcinated with Vertisol-soil.

The morphology of each sample was observed by an HR-TEM, even though the morphology is not so clear, that shows in Ag/TiO_2 by other authors like sphere [14], because composites were synthetized with clays and the nanoparticles of Ag and TiO_2 are into the soil interlayers [15]. The HR-TEM micrographs show the diameter of the Ag nanoparticles in the range of 5-20 nm, TiO_2 nanoparticles is between 15-20 nm in diameter (Figure 6b), in good agreement with the broadened diffraction peaks of TiO_2 nanoparticles in the X-Ray patterns. The size particle of natural-soil is not measured, but the size of clays are known with a nanometric size. The size particle was determinate directly from the images using the software of the equipment Digital Micrograph Gatan (™). The size particle of the compounds (Ag-NP, TiO_2-NP, and soil or clay) of the composites confirm the nanomaterial composite obtaining and, the size nano permitted the name nanocomposite.

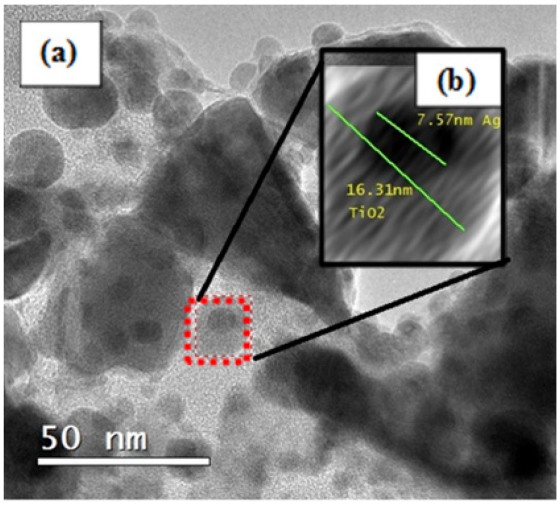

Figure 6. HR-TEM micrograph. (a) Nanocomposites 7NC synthesized-calcinated with Vertisol-soil and (b) diameters of TiO_2 and Ag nanoparticles.

Table 1 shows the morphological and structural properties of nanocomposite synthesized with Vertisol-soil (7NC) obtained by the software mentioned before and confirmed with the JCPDS cards.

Table 1. Properties of the nanocomposite synthesized with Vertisol soils.

Properties	Materials		
	Ag-NP	TiO_2-NP	SiO_2-soil-NP
Crystalline phase	face-centered-cubic	anatase	
Space group	F m -3 m (225)	I 41/a m d (141)	P 32 21 (154)
Crystal system	cubic	tetragonal	trigonal, hexagonal axes
Cell parameters Å	a=4.088	a=3.7850 c=9.5740	a=4.916 c=5.4048
d (Å) (hkl) 2θ(º)	2.36(111) 38.1	3.51(101) 25.25	3.34(011) 26.63
	2.044 (200)	1.89 (103)	4.25 (106)
	1.440 (220)	2.37 (004)	1.81 (112)

The micrographic of fast Fourier Transformed (FFT) shows the interplanar crystal spacing of 0.277 nm corresponds to the (2 0 0) plane and the d spacing of 0.236 nm correspond to the (1 1 1) plane of face-centered cubic Ag [16]; whereas the interplanar crystal spacing of 0.252 nm corresponds to the (1 0 1) plane of anatase TiO_2 phase (Figure 7b), on red and green respectively. Other authors showed the interplanar crystal spacing of 0.231 nm for Ag and 0.324 nm for TiO_2 but their composite is Ag_2O/TiO_2 on graphene platelets and for preparation of composite Ag-modified GO-TiO_2 the (1 1 1) plane was found and other d spacing to the other plane (1 0 4) [17].

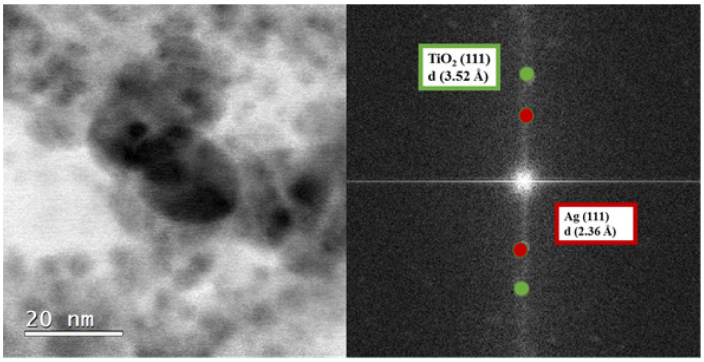

Figure 7. STEM micrograph. (a) Nanocomposite 7NC synthesized-calcinated with Vertisol-soil and (b) FFT lattice of TiO_2 on green and lattice of Ag on red.

The selected area of electron diffraction (SAED) pattern indicated that the TiO_2-NP and clays had good crystallinity (Figure 8).

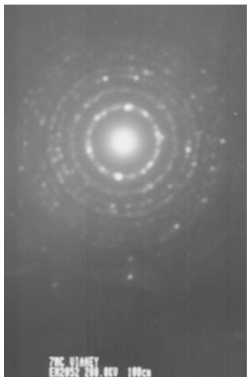

Figure 8. TEM micrograph of the Nanocomposite 7NC synthesized-calcinated with Vertisol-soil.

The SEM micrograph of the nanocomposite Ag-NP/TiO_2-NP/natural-soil-NP/exhausted coffee-ground is examined (Figure 9). On the surface, it can be seen only the natural-soil; for this reason, it cannot check the morphologies and size of the as-synthesized composites and the calcinated composites.

The chemical compositions of all synthesized products obtained by the EDS analyses are also presented in Figure 9 and show the presence of Si, Al, Ti and Ag in both composites. These results suggested that silver and TiO_2 were incorporated into the layer of natural-soil structure by the impregnation and ion exchange. There are other cations like K, Na and Ca that are part of the soil.

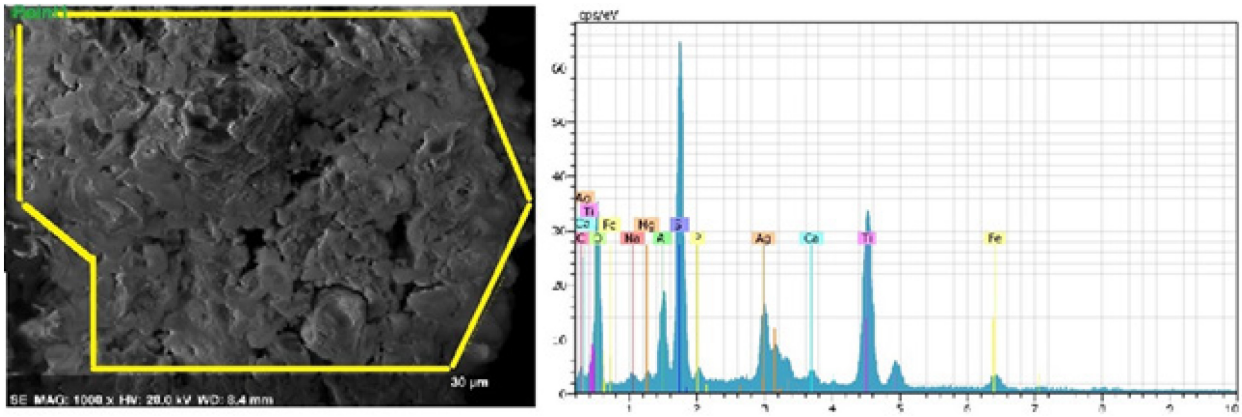

Figure 9. SEM-EDS micrograph of the nanocomposite 7NC synthetized with Vertisol-soil.

UV–vis absorption spectra analysis

The UV–vis DRS of the two material composites were obtained at room temperature using an Agilent equipment in the wavelength range of 300–800 nm. The data UV–vis spectra were processed with Microsoft Excel software, consisting of calculation of the Kubelka–Munk function, F(R∞), Eq. (1), which was extracted from the UV–vis DRS reflectance. The edge energy (Eg) for allowed transitions was determined by finding the intercept of the straight line in the low- energy rise of the plot of [F(R∞)hυ]2, for the direct allowed transition, vs. hυ, where hυ is the incident photon energy.

Diffuse reflectance Kubelka-Munk, Function F(R)

$$[F(R)x\ hv]n \approx B(hv-Eg) \quad (1)$$

where Eg is the optical band gap energy of the material, B is a material-specific constant.
The optical band gaps (Eg) of the material were obtained from the Tauc's formula (Eq. 2)

$$(\alpha hv)^{\wedge}n=K(hv-Eg) \quad (2)$$

The UV–Visible diffuse reflectance spectra of material Ag-NP/TiO_2-NP/Vertisol-soil-NP/ exhausted coffee ground (7NC) composite are shown in Figures 10, where an excitation edge at 404 nm and 2.6 eV band gap were obtained. The SPR band of composite 7NC appears at 319 nm. The adsorption energies 2.91 eV on composite 7NC surface on their Ag-NP coated by their anatase phase of TiO_2-NP and attached by soil-NP are in the range of 2.6 to 2.9 eV and the absorption coefficients

are k=0.84 and k=0.8104, respectively; comparing the results with Ag-NP (k=0.059, band gap 3.4 eV) and TiO_2-NP (k=0.072, band gap 3.2 eV), Ag/TiO_2 (k=0.145 band gap= 2.81eV a 500 °C) Pt/TiO_2 (band gap 3.13 eV), and bentonite/TiO_2-NP/AgNP composite reported a 3.05 eV band gap and k=0.017, k values increased considerably, but band gap values are lower than those reported in literature. The band gaps reduction respect to only TiO_2 (3.2 eV) or Ag/TiO_2 composites can produce superoxide radicals and hydroxyl radicals; these reactive oxidative species enhance the degradation of contaminants of emerging contaminants (ECs).

Figure 10 indicates strong interactions between nanoparticles and surfaces. The principal reason of this event is that the interfacial bonds between the interlayer of natural-soil and Ag-NP (1 1 1) and anatase phase TiO_2-NP (1 0 1) permitted a better light absorption ability of 7NC composite.

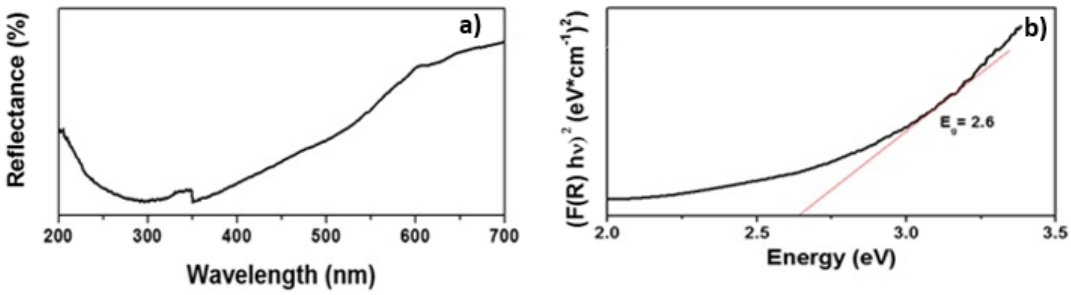

Figure 10. UV–vis DRS spectra of the 7NC material (a), and UV-Tauc plot with their respective band gap energies (b).

The band-edge energy as a result of quantum confinement and band-edge energy in semiconductor nanocrystals (Figures 10a and 10b), as could be seen on the pattern of SAED (Figure 8a). The possible origin of the increased optical band gap (Eg) in composite 7NC with Vertisol-soil is the decrease in particle size, like shows the particle size calculated by Gatan™ software previously.

FT-IR and Raman analyses

Infrared and Raman spectra of the 7NC composite were recorded in solid-state. All samples are exhibiting a complicated structure due they have natural soil-NP (Vertisol soils), Ag-NP, TiO_2-NP and exhausted coffee ground. FT-IR and Raman analyses permitted the identification of the main molecular groups present in the samples. FT-IR and Raman are useful tools for nondestructive characterization.

Figure 11 shows the FT-IR spectra of materials composites synthesized with Vertisol-soil (7NC). There are rather similar bands with some frequency shifts. In Figure 11, the 7NC nanocomposite has strong bands related to the presence of bound water (around 3400 cm^{-1}). The water might be bound to hydraulic compounds, like silicate and aluminate hydrates.

In Figure 11, the band observed at 3500 cm^{-1}, corresponding to the stretching vibration of the hydroxyl group O-H of the TiO_2-NP [18]. The band observed around 1630 cm^{-1} [19] in this work 1615 cm^{-1} corresponding to bending modes of water Ti-OH the band at 1383 cm^{-1} is not clear in this work.

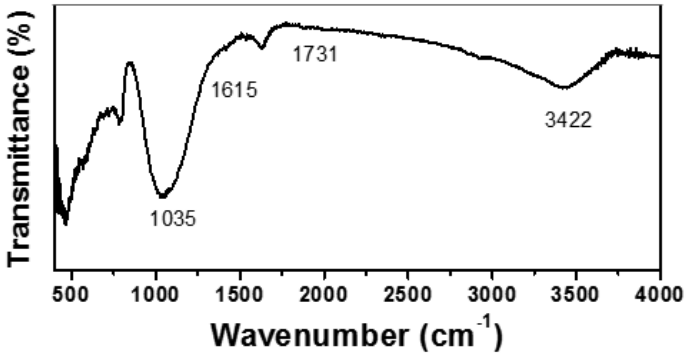

Figure 11. FT-IR spectra of the nanocomposite with Vertisol-soil (7NC).

The bands at 1040, 799, 525 and 462 cm^{-1} indicate the presence of silicate phases (Si–O vibrations) when the composites were treated at 500 ºC [19] in this work the bands at 1042, 799, 520 and 460 cm^{-1} for nanomaterial composite 7NC (Figure 12a), but strong sharp are missing in the Raman spectrum of amorphous SiO_2 (Figure 12b, Table 2). Furthermore, the spectra of FT-IR the crystalline β quartz exhibit the major band at 1080 cm^{-1} in this work 1042 cm^{-1} referring to antisymmetric Si O Si stretching vibration as witnessed in Figure 12a for composite 7NC.

Figure 12a shows the Raman spectrum of crystalline silicon contains one sharp peak at 520 cm^{-1} but if the peak shifted to below than 520 cm^{-1} is a nanocrystalline silicon structure, in this work the peak shifted at 419 cm1 in composite 7NC (Figure 12b), then the spectrum is nano-crystalline silicon (Table 3) [21]. In these nanocomposites there is another band at 632 cm^{-1} at the spectrum in this work 625 cm^{-1} correspondings to the stretching vibration of the vermiculite [19] in nanomaterial composite 7NC (Figure 12b).

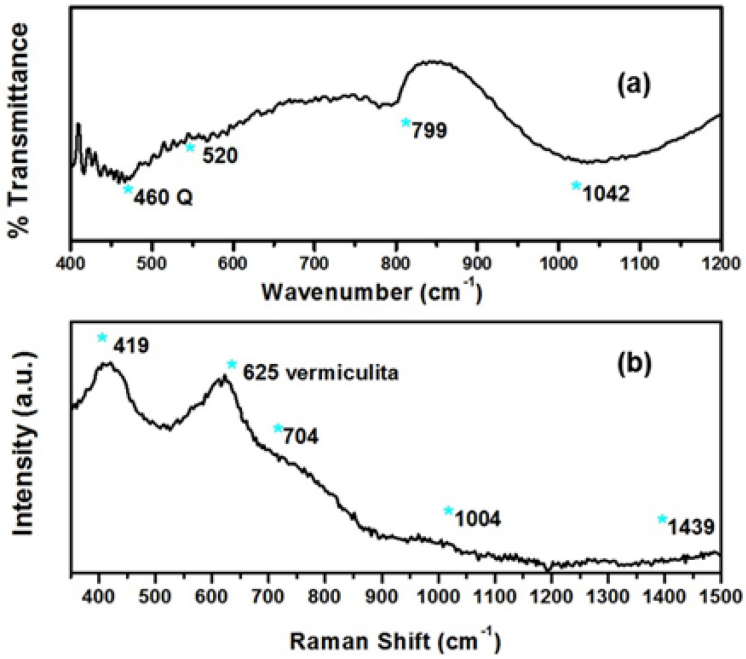

Figure 12. FT-IR and Raman spectra of the nanocomposites 7NC. (a) FT-IR spectra of SiO_2, (b) Raman spectra of SiO_2.

Table 2. Vibrational frequency assignments (FT-IR) for Si-O-Si and TiO_2.

	Si-O-Si					TiO_2		
	υ1	υ2	υ3	υ4		υ1 Ti-OH	υ2 Ti-O	υ3 Ti-O-Ti
Reference [18]	1040	799	525	462	Reference [20]	1594	1082	474
Reference [19]	1080	790			This work	1593	1084	472
This work	1042	799	520	460				

Figure 13a shows the bands at 1593, 1084, and 472 cm^{-1} to corresponded to the TiO_2 phase anatase [21]. Figure 13b shows the Raman spectrum for the nanomaterial 7NC which presents different Raman active modes with monoclinic TiO_2 phase with the C2/m group and the bands observed between 400 to 600 cm^{-1} that should be corresponding related to Ti-O modes (Eg(1), Eg(2), Eg(3) and Ag(1)) at 143, 637, 196 and 514 cm^{-1} respectively in Raman spectra [20] in this work at 145, 639, 201 and 520 cm^{-1} (Figure 13b, Table 3).

Table 3. Vibrational spectroscopic data Raman (band positions in cm^{-1}) and their tentative assignment for Si-O-Si, Ti, and Ag.

	Si-O-Si					TiO_2			
						active modes			
	υ1	υ2	υ3	υ4		Eg(1)	Eg(2)	Eg(3)	Ag(1)
Reference [18]	1092		1437	716	Reference [22]	143	637	196	514
This work	1004		1439	704		145	639	201	520

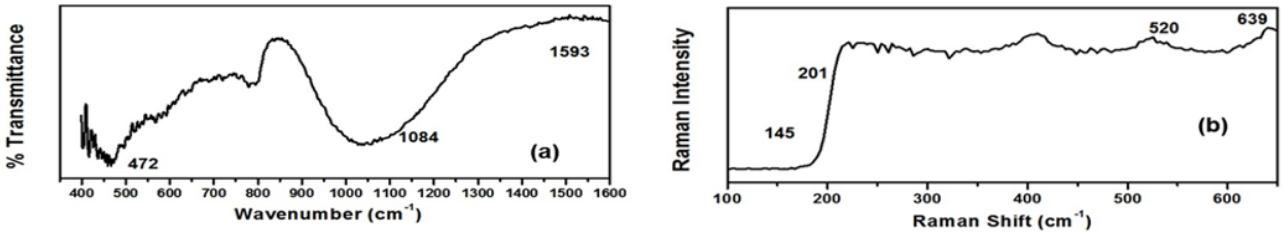

Figure 13. FT-IR (a) and Raman spectra (b) of the nanocomposites 7NC.

The Raman spectrum of AgNP displays bands shifted weak and mixed with other bands of hydroxyl OH [23]. For the mechanism of synthesis of the materials composites, the band observed at 3422 cm^{-1} proposes the presence of hydroxyl groups while those noted at 1035, 1719 and 1609 cm^{-1} in this work 1035,1731 and 1615 cm^{-1} were ascribed to alcohol groups, carbonyl stretching vibrations and the asymmetric stretching of carboxylate, corresponding with the (Figure 11) [22].

XPS analysis

XPS analyses of the silver, titanium, oxygen, and silicon-containing in composite synthesized using Vertisol-soil (7NC) as the titanium source and silver source were carried out to determine surface composition and oxidation states of the active metals (Figure 14).

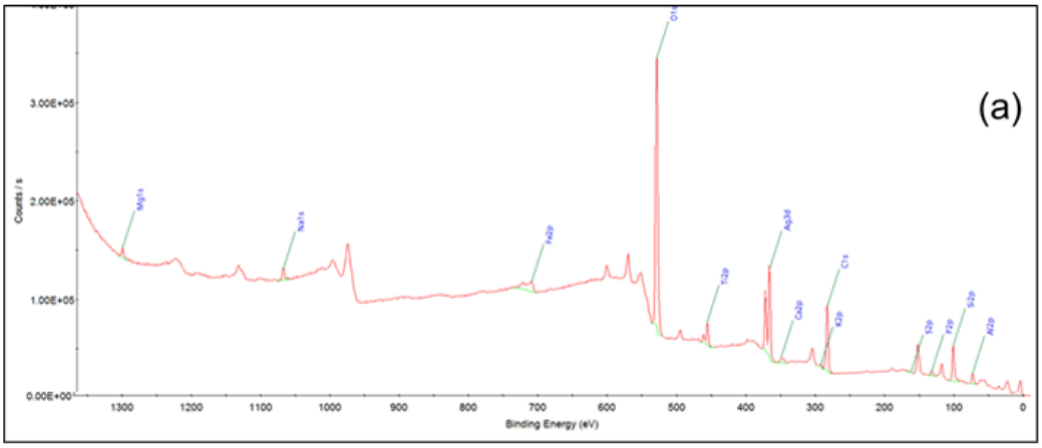

Figure 14. XPS spectra of the nanocomposite with Vertisol-soil (7NC).

The XPS Ag 3d spectrum of those composites exhibit the binding energy of Ag 3d5/2 line at 368.09 eV to composite 7NC with Vertisol-soil that is characteristic of Ag with oxidation state (0), in agreement with the kinetic energy of Ag M5N45N45 Auger peak at 357.7 eV [24] Figure 15a shows that the nanomaterial with Vertisol-soil exhibit the binding energy of Ag 3d5/2 line at 368.09 eV.

Natural soil and exhausted coffee ground mixed with ethanol contain extensive numbers of hydroxyl groups that can act as good chemical reductants (Figure 15 b). The presence of this functional group in the synthesis process allows the formation of metal nanoparticles. The sequestration of cations $[Mn^{+}]$ or hydroxylated cations $[M(OH)]m^{+}$ that bear nucleation or growth processes are accelerated by the highly reactive hydroxyl groups presented in natural-soil and coffee

ground. After hydrothermal process when calcinated at 500 ºC which removes via combustion of their organic frame formed the TiO_2-NP anatase phase giving rise to the formation of dispersed oxides, can be seen on graphics of XPS (Figure 15), the oxidations states of Ag 3d is present, oxidation states of Ti^{4+}, Figure 15c for nanocomposite 7NC where centers were formed creating shallow and deep trap states, reduce the band gap and inducing separation of photo-induced charge pairs, the electrons and the holes are presented in the nanocomposites 7NC which permitted the enhancement on catalyst activity [25, 33].

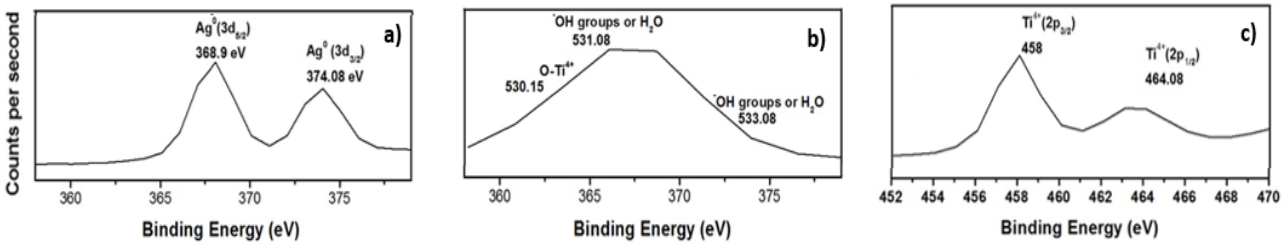

Figure 15. High resolution XPS spectra of (a) Ag 3d of the nanocomposite with Vertisol-soil (7NC), (b) O 1s of the nanocomposite with Vertisol-soil, and (c) Ti 2p of the nanocomposite with Vertisol-soil.

The presence of Ag 3d (Figure 15a) allowed confirm the reason about the composite 7NC has an antimicrobial activity and the formation of the Schottky barrier is only possible when silver transition metal is present in its elemental state (0) which has been confirmed from XPS analysis this permitted the enhancement on catalyst activity and, as result the enhancement on antimicrobial activity [26].

Antimicrobial activity of the nanocomposite Ag-NP/TiO_2-NP/natural-soil-NP/exhausted coffee-ground.

Screening of antimicrobial activity by Disk Diffusion Method, which is based on the outset of alive bacteria can grow into a colony. The antimicrobial activity is evidenced by an inhibition zone of bacteria *E. coli* and bacteria *S. aureus* growth around the composites of Ag-NP/TiO_2-NP/natural-soil NP/exhausted coffee ground with Vertisol-soil (7NC), as shown in Figure 16. No bacterial growth was observed on the top of and adjacent to the nanomaterial composite for Ag-NP/TiO_2-NP/natural-soil-NP/exhausted coffee ground. The result demonstrates that all the composites could inhibit bacterial growth. The time-dependent durability of the synthesized Ag-NP/TiO_2-NP/natural-soil-NP/exhausted coffee-ground (7NC) composite was also been studied for different time intervals, and the diameters of inhibition of nanocomposite 7NC was 17 (0.05) mm in two bacteria. It was found that Ag-NP/TiO_2-NP/Vertisol-soil-NP/exhausted coffee-ground (7NC) inhibited and suppressed the bacteria, other authors presented ZOI=25 mm for the composite of Ag deposited into TiO_2-NP [27] or a ZOI of 4 mm for the composite Ag deposited on MMT for S. aureus and is not able for inhibition of *E. coli* [28].

The effect in which are created hydrophilic OH groups on illuminated via UV light irradiation TiO_2 surface is well known. The loading of silver does not affect the photoinduced hydrophilicity of TiO_2, but the result reveals that two composites could inhibit bacterial growth (Figure 16). The great antimicrobial activity of the composites under the UV light is due to the synergistic antimicrobial effects of the photocatalytic reaction of the TiO_2 coating and silver.

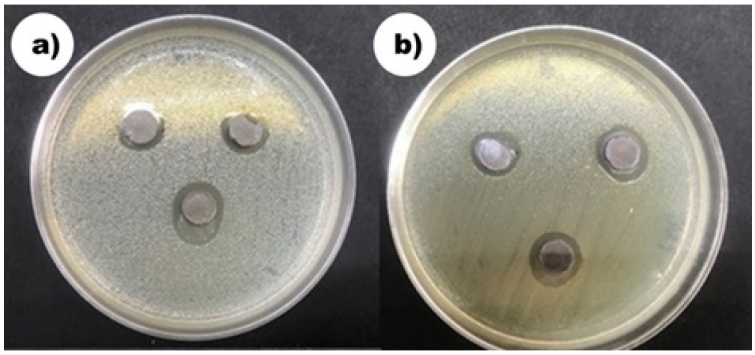

Figure 16. Antimicrobial activity of the synthesized materials. (a) Nanocomposite with Vertisol-soil 7NC against *E. coli*, or against *S. aureus* (b).

The enhanced antimicrobial activity of irradiated composites is attributed to the production of reactive oxygen species (ROS) by the release of metal ions (Ag^+ in this work), which are produced by the presence of Ag3d (Figure 15a). The formation of the Schottky barrier is only possible when metal is present in its elemental state which has been confirmed from XPS analysis; this permitted the enhancement of catalyst activity [26].

Photocatalytic of nanocomposites synthesized with Vertisol-soil on MB degradation.

The degradation reaction kinetics of the dyes with and without photocatalyst was monitored by collecting UV/Vis spectra after a regular interval of times (30 minutes). Figures 17 show a series of absorbance spectra of MB with initial concentration using composite 7NC as a photocatalyst respectively. The graphics show the range of 500 to 800 nm and the two major absorption peaks appear at λ=612 and 664 nm which are characteristic of MB and when it exposed to UV light the absorbance reduced with increasing exposure time and dye degradation identified by color change indicating photocatalytic activity of 7NC composite. In this experiment the pH of the solution was not controlled. It has been reported that at a greater surface area, the photocatalysis increases [29]. The nanocomposite 7NC (Figure 17) had 18.41 m^2g^{-1}.

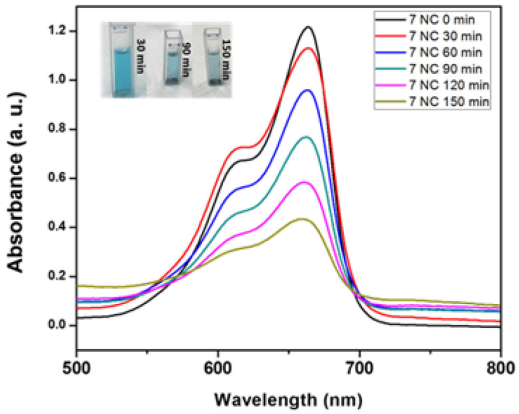

Figure 17. Variation in MB dye concentration with sunlight irradiation time in the presence of Ag-NP/TiO_2-NP/Vertisol-soil-NP/exhausted coffee-ground (7NC).

Figure 18 shows the kinetics analysis of reactions in the nanocomposites 7NC. The photocatalytic degradation of MB dye was inclined by the percentage of this degradation of MB dye in 150 minutes (64.99%) obtained for the nanocomposite 7NC. Our material was not better that another nanocomposite with carbon dots (CDs), Ag and TiO_2-NP with commercial name P25. CDs/Ag/P25 where exhibited a photocatalytic performance in MB degradation (100% degradation within 15 min) under UV light [30], even whit a reported surface area of 62.5 m^2 g^{-1}. The photocatalytic kinetics (Figure 18b) was studied using Langmuir-Hinsheldwood equation for calculated the rate constant of degradation of MB, k (min^{-1}) under UV light. The values of the rate constant for the nanocomposite

synthetized with Vertisol-soil (7NC) was 0.0069 min^{-1}. [30]. The rate constant of nanocomposites synthetized is lower than reported e.g. composite Ag-TiO_2-Bentonite k=0.055 min^{-1} under UV-light and reported 119 m^2g^{-1} in their surface area [25]. The improvement enhanced of catalytic activity requires a material with large surface area and that metals doped could be into the interlayers but closed to the surface among other features [25].

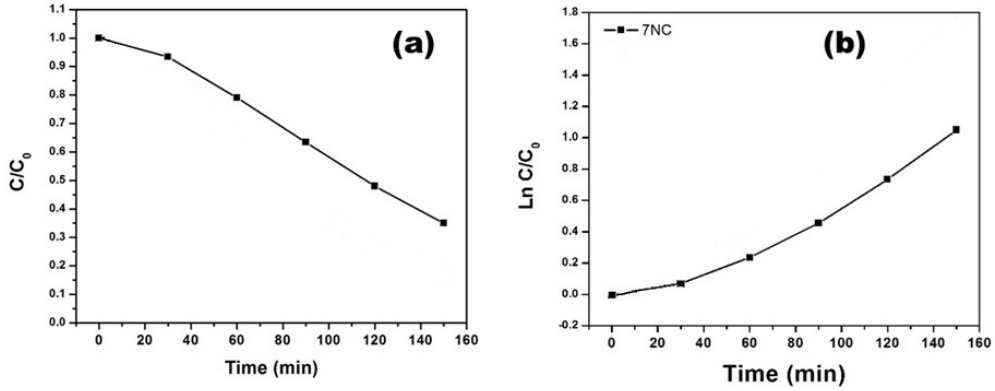

Figure 18. Kinetics of decomposition of MB by the photocatalysts of the nanocomposite Ag-NP/TiO_2-NP/Vertisol-soil-NP/exhausted coffee-ground (7NC).

Nitrogen-adsorption isotherms, surface areas, and pore volumes.

The surface area of the nanocomposite Ag-NP/TiO_2-NP/vertisol-soil-NP/exhausted coffee-ground (7NC) was 17.56 m^2g^{-1}, the types of soil are better surface area than nanomaterials synthesized (Table 4), but some works reported that TiO_2-NP are 42.6 m^2 g^{-1} is in this context the photocatalytic process is lower than this work 90 minutes to dye MB [22], when had a Ag/TiO_2 with bentonite composite the surface area is 119 m^2 g^{-1} the catalyst loading was 0.1 g L^{-1} and not reported the surface area [25].

Table 1. BET Surface area and pore volume of used soil and nanocomposite.

Material	**Surface area (m^2g^{-1})**	**Pore volume (cm^3g^{-1})**
Vertisol soil, from Guanajuato, Mexico	18.4190	0.000128
Ag-NP/TiO_2-NP/Vertisol-soil-NP/exhausted coffee-ground	17.5678	0.0020

All isotherms of adsorption and desorption curves for types soils and nanomaterials synthesized show a type III isotherm and hysteresis loops typical a microporous material (Figure 19).

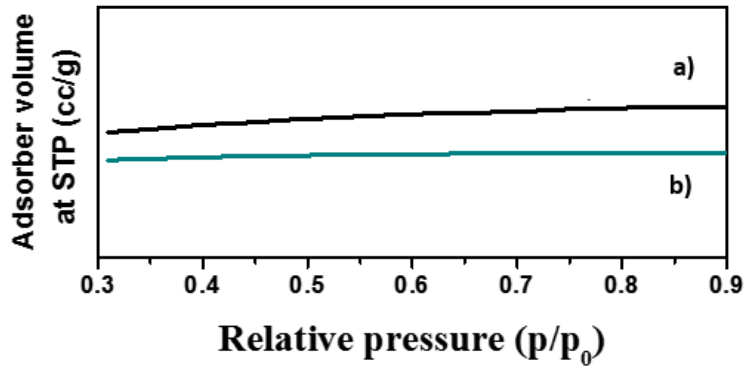

Figure 19. Isotherms graph. (a) Nanocomposite 7NC synthetized with vertisol-soil, and (b) Vertisol-soil.

The nanocomposite synthesized with the Vertisol-soil (7NC) could have facilitated the adsorption of a greater number of dye molecules (methylene blue). Then the photo-generated electrons and holes will be increased, and the electron will react with O_2 to produce O_2^- increased and improvement photocatalytic activity

Conclusions

Clays from a vertisol soil were used to synthesis a nanocomposite with Ag- and TiO_2-nanoparticles and exhausted coffee ground. The nanocomposite was fully characterized by cutting-edge scientific equipment, and according to the results, it can degrade the organic pollutant methylene blue. Also, the nanocomposite has antimicrobial activity and could dissipate other harmful chemicals. Besides, this nanocomposite can also be used to chelate and separate other contaminants from soil or water, as witnessed by FT-IR and RAMAN characterization.

Acknowledgments

This research was founded by 'Ciencia Básica SEP-CONACyT' project 287225, 'Fondo FONCYT-COECYT-Convocatoria 2019-C13, Efecto de Nanopartículas de Uso Agrícola sobre el Desarrollo de la Planta de Maíz (Zea mays L.) y las Propiedades Fisicoquímicas y Biológicas del Suelo (COAH-2019-C13-C006)', the Sustainability of Natural Resources and Energy Programs (Cinvestav-Saltillo), and Cinvestav Zacatenco. Urdapilleta-Inchaurregui is grateful for postgraduate fellowship trough CONACYT as well as for CINVESTAV-IPN. Special thanks for D. Bahena, J. Roque, M. Guerrero Fuentes for their technical support (STEM, SEM, and XRD analyses).

References

[1] L. Joseph, Byung-Moon Jun, Min Jang, C. Min Park, J. C. Muñoz-Senmache, A. J. Hernández-Maldonado, A. Heyden, Miao Yu, Y. Yoon, Removal of contaminants of emerging concern by metal-organic framework nanoadsorbents, Chem. Eng. J. 369 (2019) 928–946

[2] K. I. Ekpeghere, W. J. Sim, H. J. Lee, and J. E. Oh, Occurrence and distribution of carbamazepine, nicotine, estrogenic compounds, and their transformation products in wastewater from various treatment plants and the aquatic environment, Sci. Total Environ. 640-641 (2018) 1015-1023.

[3] M. K. Uddin, A review on the adsorption of heavy metals by clay minerals, with special focus on the past decade, Chem. Eng. J. 308 (2017) 438–462

[4] Andrea Pérez-Moreno, Cesar Roberto Sarabia-Castillo, Gabriela Medina-Pérez, Hermes Pérez-Hernández, Jorge Roque De La Puente, Sirenia González-Pozos, Langen Corlay-Chee, Angelina Chamizo-Checa, Rafael G. Campos-Montiel, Fabián Fernández-Luqueño. Nanomaterials modify the growth of crops and some characteristics of organisms from agricultural or forest soils: An experimental study at laboratory, greenhouse and land level. Mexican J. Biotech. 4 (2019) 29-49

[5] S. Yazici Guvenc, B. Alan, E. Adar, and M. S. Bilgili, The impact of nanoparticles on aerobic degradation of municipal solid waste, Waste Manag. Res. 35 (2017) 426–436.

[6] J. Pérez-Carvajal, P. Aranda, S. Obregón, G. Colón, and E. Ruiz-Hitzky, TiO_2-clay based nanoarchitectures for enhanced photocatalytic hydrogen production, Microporous Mesoporous Mater. 222 (2016) 120–127

[7] H. P. Qi, H. L. Wang, D. Y. Zhao, and W. F. Jiang, Preparation and photocatalytic activity of Ag-modified GO-TiO_2 mesocrystals under visible light irradiation, Appl. Surf. Sci. 480 (2018) 105–114

[8] T. S. Wu, K. X. Wang, G. D. Li, S. Y. Sun, J. Sun, and J. S. Chen, Montmorillonite-Supported Ag/TiO_2 nanoparticles: An efficient visible-light bacteria photodegradation material, ACS Appl. Mater. Interfaces 2-2 (2010) 544–550

[9] Y. Poo-arporn et al., Photocatalytic oxidation of thiophene over cerium doped TiO_2 thin film, Mater. Sci. Semicond. Process. 93 (2018) 21–27

[10] I. Khan, K. Saeed, and I. Khan, Nanoparticles: Properties, applications and toxicities, Arabian Journal of Chemistry, Elsevier B.V., (2017)

[11] Wayne Institute, Clinical and Laboratory Standards Institute. Performance Standards for Antimicrobial Disk Susceptibility Tests; Approved Standard, 2012 Eleventh Edition, vol. 32, no. 1

[12] USEPA, National Primary Drinking Water Regulations Contaminant MCL or TT, 1, (2009) 1-10.

[13] S. OPdl. and Paho/WHO, Prueba de Difusión por Disco, chapter 4 PAHO/WHO (2010) 39–52

[14] Y. Liu, C. Hou, T. Jiao, J. Song, X. Zhang, R. Xing, J. Zhou, L. Zhang and Q. Peng, Self-assembled AgNP-containing nanocomposites constructed by electrospinning as efficient dye photocatalyst materials for wastewater treatment, Nanomaterials, 8-35 (2018) 1-14

[15] P. Makal and D. Das, Self-doped TiO_2 nanowires in TiO_2 -B single phase, TiO_2 -B/anatase and TiO_2 -anatase/rutile heterojunctions demonstrating individual superiority in photocatalytic activity under visible and UV light, Appl. Surf. Sci. 455 (2018) 1106–1115

[16] X. Yao, X. Liu, and X. Hu, Synthesis of the Ag/AgCl/g-C_3N_4 composite with high photocatalytic activity under visible light irradiation," ChemCatChem, 6 (2014) 3409–3418

[17] R. Saleh, A. Taufik, and S. P. Prakoso, Fabrication of Ag_2O/TiO_2 composites on nanographene platelets for the removal of organic pollutants: Influence of oxidants and inorganic anions, Appl. Surf. Sci. 480 (2019) 697–708

[18] A. León, P. Reuquen, C. Garín , R. Segura , P. Vargas, P. Zapata and P. A. Orihuela, FTIR and raman characterization of TiO_2 nanoparticles coated with polyethylene glycol as carrier for 2-methoxyestradiol," Appl. Sci. 7-1 (2017) 1–9

[19] S. Gunasekaran and G. Anbalagan, Spectroscopic study of phase transitions in natural calcite mineral, Spectrochim. Acta - Part A Mol. Biomol. Spectrosc. 69-4 (2008) 1246–1251

[20] C. E. Fischer, J. Mink, L. Hajba, Z. Bacsik, C. Németh, J. Mihály, A. Raith, M. Cokoja, F. E. Kühn, Vibrational spectroscopic study of SiO_2 -based nanotubes, Vib. Spectrosc. 66 (2013) 104–118

[21] K. H. Kim, D. J. Lee, K. M. Cho, S. J. Kim, J. K. Park, and H. T. Jung, Complete magnesio thermic reduction reaction of vertically aligned mesoporous silica channels to form pure silicon nanoparticles, Sci. Rep. 5 (2015) 1–7

[22] K. S. Saranya, V. V. T. Padil, C. Senan, R. Pilankatta, K. Saranya, B. George, S. Wacławek and Miroslav ˇCerník, Green synthesis of high temperature stable anatase titanium dioxide nanoparticles using gum kondagogu: Characterization and solar driven photocatalytic degradation of organic dye. Nanomaterials, 8 (2018) article number 1012

[23] K. Logaranjan, A. J. Raiza, S. C. B. Gopinath, Y. Chen, and K. Pandian, Shape- and size-controlled synthesis of silver nanoparticles using *Aloe vera* plant extract and their antimicrobial activity, Nanoscale Res. Lett., 11-1, (2016) Article number 520

[24] Y. L. Mikhlin et al., On the nature of citrate-derived surface species on Ag nanoparticles: Insights from X-ray photoelectron spectroscopy," Appl. Surf. Sci. 427 (2018) 687–694

[25] A. Mishra, A. Mehta, S. Kainth, and S. Basu, Effect of different plasmonic metals on photocatalytic degradation of volatile organic compounds (VOCs) by bentonite/M-TiO_2 nanocomposites under UV/visible light, Appl. Clay Sci. 153 (2017) 144–153

[26] M. R. Khan, T. W. Chuan, A. Yousuf, M. N. K. Chowdhury, and C. K. Cheng, Schottky barrier and surface plasmonic resonance phenomena towards the photocatalytic reaction: Study of their mechanisms to enhance photocatalytic activity, Catal. Sci. Technol. 5 (2015) 2522–2531

[27] B. Yu, K. M. Leung, Q. Guo, W. M. Lau, and J. Yang, Synthesis of Ag-TiO_2 composite nano thin film for antimicrobial application, Nanotechnology. 22 (2011) 2–11

[28] D. Louise, S. Bonga, M. Manna, F. B. Pinto, M. Fatima, and T. Tayad, Synthesis and Characterization of Silver Nanoparticles Anchored on Montmorillonite via Chemical Reduction, Int. J. Sci. Eng. Res. 7 (2016) 30–37

[29] A. Gołabiewskaa, W. Lisowski, M. Jarek, G. Nowaczyk, M. Michalska, S. Jurga, A. Zaleska-Medynska, The effect of metals content on the photocatalytic activity of TiO_2 modified by Pt/Au bimetallic nanoparticles prepared by sol-gel method, Mol. Catal. 442 (2017) 154–163

[30] C. Wang, K. Yang, X. Wei, S. Ding, F. Tian, and F. Li, One-pot solvothermal synthesis of carbon dots/Ag nanoparticles/TiO_2 nanocomposites with enhanced photocatalytic performance, Ceram. Int. 44 (2018) 22481–22488

[31] P. Khwanmuang, P. Rotjanapan, A. Phuphuakrat, S. Srichatrapimuk, and C. Chitichotpanya, In vitro assessment of Ag-TiO_2/polyurethane nanocomposites for infection control using response surface methodology, React. Funct. Polym. 117 (2017) 120-130

[32] L. Liu, H. Bai, J. Liu, and D. D. Sun, Multifunctional graphene oxide-TiO_2-Ag nanocomposites for high performance water disinfection and decontamination under solar irradiation, J. Hazard. Mater. 261 (2013) 214–223

[33] L. Gharibshahi, E. Saion, E. Gharibshahi, A. H. Shaari, and K. A. Matori, Structural and optical properties of Ag nanoparticles synthesized by thermal treatment method, Materials (Basel). 10 (2017) article number E402